frontiers in Earth Science

ORIGINAL RESEARCH
published: 04 December 2019
doi: 10.3389/feart.2019.00322

Geochronology and Depositional History of the Sandy Springs Aeolian Landscape in the Unglaciated Upper Ohio River Valley, United States

Matthew P. Purtill[1], J. Steven Kite[2] and Steven L. Forman[3]*

[1] Department of Geology and Environmental Science, State University of New York at Fredonia, Fredonia, NY, United States, [2] Department of Geology and Geography, West Virginia University, Morgantown, WV, United States, [3] Department of Geosciences, Baylor University, Waco, TX, United States

The study of active and stabilized late Quaternary aeolian landforms provides important proxies for past climate events and environmental transitions. Despite an overall increase in the study of aeolian landforms in previously glaciated and coastal settings in eastern North America, the history of aeolian sedimentation in many unglaciated inland alluvial settings remain poorly understood. This study reports on the geochronology and depositional history of aeolian landforms and sediments in the unglaciated upper Ohio Valley at the Sandy Springs site. Aeolian landforms and sediments include complex, linear, barchan-like, and climbing dunes; an interdune sand sheet; and sandy loess that blankets high valley surfaces. At Sandy Springs, aeolian dune sands and sandy loess are restricted to intermediate (S2) and higher (S3) geomorphic surfaces. Eight optically stimulated luminescence age estimates constrain the initiation of aeolian processes on the S2 surface to sometime after 17 ka and episodic deposition on the S2 and S3 surfaces between 11 and 1.4 ka. The distribution of aeolian sediments at Sandy Springs is influenced by several past factors including local wind fetch potential, sediment availability, and underlying alluvial topography. Sediment availability is interpreted as the primary factor controlling aeolian processes and appear linked to several pan-regional paleoclimate events. Sandy loess deposition at ca. 8.2 ka on the S3 surface may reflect hydrologic variability and cooling, associated with the final pulse of meltwater into the North Atlantic from the Laurentide Ice Sheet. Dune reactivation and erosion at ca. 4.5 ka on the S2 surface indicate enhanced sediment availability possibly associated with drought conditions. These results illustrate that the deciphering the coupled fluvial-aeolian records in this catchment of the Ohio River provides new insight into the nature of changing surface processes against the backdrop of climate variability over the past ca. 20 ka.

Keywords: aeolian deposition, fluvial-aeolian interaction, OSL dating, geochronology, paleoclimate, late Quaternary, Ohio River Valley

OPEN ACCESS

Edited by:
Gary E. Stinchcomb, Murray State University, United States

Reviewed by:
Andrea Zerboni, University of Milan, Italy
Mingrui Qiang, South China Normal University, China

****Correspondence:***
Matthew P. Purtill
matthew.purtill@fredonia.edu

Specialty section:
This article was submitted to Quaternary Science, Geomorphology and Paleoenvironment, a section of the journal Frontiers in Earth Science

Received: *20 September 2019*
Accepted: *19 November 2019*
Published: *04 December 2019*

Citation:
Purtill MP, Kite JS and Forman SL (2019) Geochronology and Depositional History of the Sandy Springs Aeolian Landscape in the Unglaciated Upper Ohio River Valley, United States. Front. Earth Sci. 7:322. doi: 10.3389/feart.2019.00322

INTRODUCTION

Over the last 30 years there has been an increase in the study of active and stabilized late Quaternary aeolian landforms and sediments in the eastern United States. Studies largely have focused on aeolian depositional processes and geochronologies of dune fields, sand sheets, sandy loess or coversands, and loess. Possible links between aeolian processes and past climatic or environmental conditions such as drought also have been explored (e.g., Muhs and Zárate, 2001; Booth et al., 2005; Willard et al., 2005; Li et al., 2007). Most aeolian research in the eastern United States has focused either on deglaciated landscapes including alluvial valleys, paleochannels, lake plains, and outwash plains (e.g., Arbogast et al., 2002; Arbogast and Packman, 2004; Rawling et al., 2008; Miao et al., 2010; Wang et al., 2011; Hanson et al., 2015) or coastal settings such as the Gulf Coastal Plain or the Atlantic Coastal Plain (e.g., Ivester et al., 2001; Ivester and Leigh, 2003; Kilibarda et al., 2014b; Forman, 2015; Markewich et al., 2015; Swezey et al., 2016). Aeolian landforms also occur in many unglaciated interior alluvial valleys (e.g., Bettis et al., 2003; Busacca et al., 2004; Markewich et al., 2015) and have the potential to yield paleoenvironmental data, help assess valley sensitivity to climate change, and reveal archeological evidence of past human activity (e.g., Wagner and McAvoy, 2004; Feathers et al., 2006; Lothrop and Cremeens, 2010; Daniel et al., 2013; Purtill and Kite, 2015). Although aeolian sediments for some unglaciated valleys in eastern United States have been described in detail including the lower Mississippi Valley (e.g., Saucier, 1977; Rodbell et al., 1997; Rittenour et al., 2007; Markewich et al., 2015), aeolian landforms in other drainages such as the upper Ohio Valley have received less attention and remain largely undated (Rutledge et al., 1975; Chappell, 1988; Simard, 1989). To achieve a better understanding of past aeolian transport and deposition cycles for the eastern North America, additional geochronology and geomorphic histories are required for interior valleys, especially ones that have received limited attention.

In this study, we describe a stabilized, vegetated aeolian system at the Sandy Springs site in an unglaciated reach of the upper Ohio Valley (**Figure 1**). A geochronology and depositional history is advanced for aeolian landforms and sediments at Sandy Springs based on geomorphic, stratigraphic, and sedimentary assessment, coupled with optically stimulating luminescence (OSL) ages on quartz grains. Furthermore, we consider possible links between paleoclimate events and aeolian processes at Sandy Springs and, through extrapolation, the broader upper Ohio Valley. This study is the first detailed geochronology and geomorphic description of an aeolian system in the upper Ohio Valley and provides new insights into the nature of interaction between aeolian, fluvial, and glacial processes in the valley.

STUDY AREA

Situated in a heavily dissected section of the Shawnee-Mississippian Plateau of the Appalachian Plateaus (Brockman, 2006), Sandy Springs is located in an unglaciated portion of the upper Ohio Valley (**Figure 1**). Regional bedrock geology includes siltstones, shales, limestones, and bedded sandstones of Silurian, Devonian, and Mississippian ages (Coogan, 1996; Slucher et al., 2006). Although unglaciated, Sandy Springs alluvial landforms resulted from fluvioglacial outwash and fine overbank sediments sourced from the Ohio and Scioto Rivers (Morris and Pierce, 1967; Pavey et al., 1999).

The valley bottom at Sandy Springs is ∼2.4 km wide and situated on a major meander of the Ohio River (**Figures 1B–D**). Aeolian sediments are located on both the north bank of the Ohio River at Sandy Springs and on the south bank in Vanceburg, Kentucky (**Figure 1D**). When mapped in total, aeolian deposits include ∼304 ha of land (Morris and Pierce, 1967; Lucht and Brown, 1994; Purtill and Kite, 2015; Purtill, 2016, 2017). Currently, pool elevation for this river reach is dam-controlled at 148 m, although early navigation charts list a low-water elevation of 141 m at Sandy Springs (Jones, 1916, p. 163). Low-water elevations are used in this study to approximate pre-dam pool averages (following Simard, 1989, pp. 21–25). A historic high-water mark of 164 m was reported at Sandy Springs during a January flood in 1937 (Morris and Pierce, 1967; NOAA, 2017).

Three separate geomorphic classifications of the Sandy Springs valley bottom have been proposed and each delineates between two and four alluvial/outwash surfaces or terraces above a modern floodplain (Morris and Pierce, 1967; Pavey et al., 1999; Purtill and Kite, 2015; Purtill, 2016, 2017). In the 1960s, the valley bottom initially was mapped as consisting of a high surface (Qo) at 185 m with an assumed Illinoian age (ca. 160 ka) and three lower fluvial surfaces (Qow) at 175, 169, and 166 m with inferred Wisconsinan ages between 70 and 15 ka (Morris and Pierce, 1967). Up to 5 m of silty sediment (Qe) interpreted as loess was reported to mantle much of the highest, assumed Illinoian, surface (Morris and Pierce, 1967).

Pavey et al. (1999) reclassified the valley bottom as only containing two outwash surfaces (O1, O2) above the modern channel at Sandy Springs. A higher fan-shaped O1 surface, which appears to represent the Qo surface, reportedly is composed of sand and gravel and interpreted as an outwash terrace. Based on topographic correlation to more northerly radiocarbon-dated moraines in central Ohio, the O1 surface is suggested to have formed during the Late Wisconsinan, ca. 22 to 18 ka (Pavey et al., 1999). This age is markedly younger than the Illinoian age assumed by Morris and Pierce (1967). The lower, expansive O2 landform contains outwash sand and gravels with an inferred age of 18 to 15 ka and appears correlative to the Wisconsinan terraces (Qow) of Morris and Pierce (1967).

Recent analysis of LiDAR data resulted in a second reclassification of the valley bottom (Purtill and Kite, 2015; Purtill, 2016, 2017). Valley-bottom morphometrics suggest four geomorphic surfaces (S0–S3) above the Ohio River's pre-lock and dam low-water elevation. This classification is adopted for this article and includes a modern floodplain (S0) separate from a low landform (S1) by an escarpment up to 6 m high. The S1 tread rises 17–21 m and is characterized by pronounced ridge-and-swale topography. A broad S2 surface occurs between 21 and 39 m, gradually slopes toward the Ohio River, and has low ridge-and-swale topography. S2 appears equivalent with both the O2 outwash terrace (Pavey et al., 1999) and Qow outwash terraces

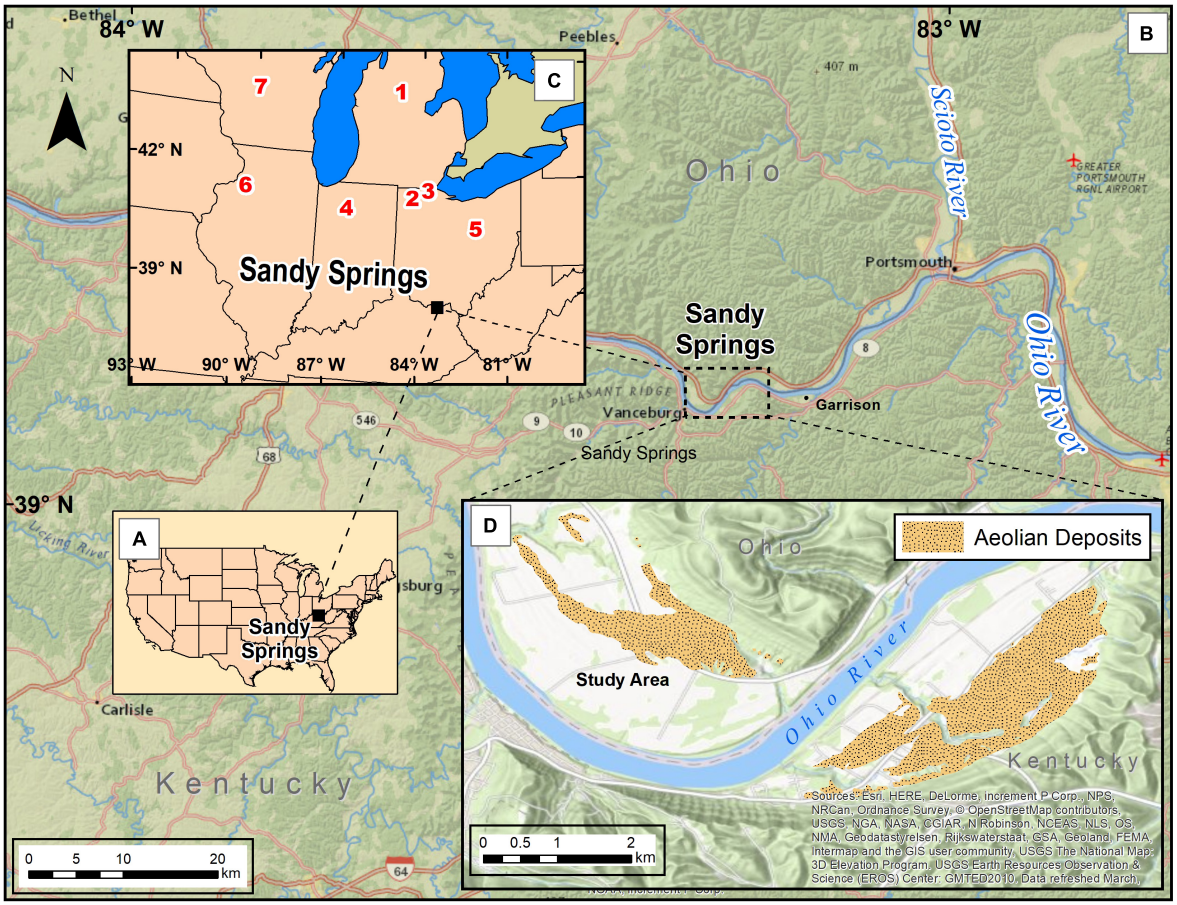

FIGURE 1 | Location of Sandy Springs **(A)** in continental United States and **(B)** showing position along the upper Ohio River in relation to the Scioto River, and **(C)** with reference to additional sites mentioned in the text (1 = Arbogast et al., 2015; 2 = Blockland, 2013; 3 = Campbell et al., 2011; 4 = Kilibarda and Blockland, 2011; 5 = Lutz et al., 2007; 6 = Miao et al., 2010; 7 = Rawling et al., 2008). **(D)** Combined distribution of sediments interpreted as aeolian in past geologic and pedologic literature (Chaplin and Mason, 1967; Morris and Pierce, 1967; USDA-NRCS, 2017). This study focuses on areas north of the Ohio River as illustrated **(D)**.

(Morris and Pierce, 1967). The S3 geomorphic surface ranges between 39 and 46 m and abuts eastward with dissected bedrock uplands. To the west, this surface is eroded and discontinuous. The S3 surface is equivalent to both the O1 outwash terrace (Pavey et al., 1999) and Qo terrace (Morris and Pierce, 1967).

Sandy Springs aeolian landforms are presently vegetated or in cultivation that includes seasonal tilling (**Figure 2**). Where undisturbed, aeolian landforms host a remnant sand-prairie vegetation of xeric plant species such as eastern prickly pear cactus (*Opuntia humifusa*), passion flower (*Passiflora incarnata*), little whitlow grass (*Draba brachycarpa*), spreading sandwort (*Arenaria patula*), and silkgrass (*Chrysopsis graminifolia*) (Vincent et al., 2011; Purtill, 2017). Pollen data from the upper Ohio Valley suggest a transition from an early savanna-like setting dominated by spruce (*Picea* sp.) and grasses during the late Pleistocene to a mixed mesophytic forest of oak (*Quercus* sp.), hickory (*Carya* sp.), maple (*Acer* sp.), chestnut (*Castanea* sp.), walnut (*Juglans* sp.), and elm (*Ulmus* sp.) by the mid-Holocene (Fredlund, 1989; Purtill, 2012, pp. 42–47).

The modern southern Ohio climate is humid subtropical with no significant precipitation shortages throughout the year (Thornthwaite, 1931; Peel et al., 2007). Average annual precipitation is 1092 mm, with the highest monthly totals between March and August, while mean annual temperature is 11.8°C (Lucht and Brown, 1994, p. 124). Records from

FIGURE 2 | General view of now vegetated hummocky landscape west of U.S. Route 52 including the area containing complex dunes and barchan-like dune.

historic water wells indicate a variable water table surface ranging between 0.5 and 1 m below surface and averaging 0.8 m (ODNR, 2017). Modern surface wind speed and direction vary seasonally. Based on 1930–1996 climatic data from stations at Lexington and Jackson in Kentucky; Cincinnati, Columbus, and Dayton in Ohio; Pittsburg, Pennsylvania; and Huntington, West Virginia; surface wind direction at Sandy Springs ranges from S to WSW with more southerly orientation during summer months and a more western orientation during winter months (National Climatic Data Center, 1996). Paleoclimatic reconstructions from late Pleistocene proxies suggest a more northerly (WNW) wind direction was typical in eastern North American during the Wisconsinan glaciation (Wells, 1983; Thorson and Schile, 1995; Kilibarda and Blockland, 2011).

MATERIALS AND METHODS

OSL Dating

Landform chronology reconstruction was based on eight samples submitted for OSL dating (Aitken, 1998) at the Geoluminescence Dating Research Lab at Baylor University. Single aliquot regeneration (SAR) protocols (Murray and Wintle, 2003) were used for OSL dating to estimate the apparent equivalent dose of the 63–44, 250–355, 355–425, and 425–500 μm quartz fractions for 28–61 separate aliquots. A full discussion of OSL methodology and results is provided in **Supplementary Material**.

Morphometric Landform Analysis

Airborne laser altimetry (LiDAR) data is the basis for morphometric analysis of discrete aeolian and alluvial landform elements (e.g., dunes, ridges, knobs, basin etc.). Data tiles at 0.762 m resolution in ESRI Grid format derive from the Ohio Geographically Referenced Information Program website (OGRIP, 2015). Sand dune classification follows established morphometric schemas (Pye, 1982; Lancaster, 2011; Thomas, 2011). In cases where sedimentary structures for dunes are identified, morphometric dune classifications are verified.

Sedimentary and Stratigraphic Descriptions

Sedimentary and stratigraphic information derives from the description and interpretation of 33 sections and 163 sediment samples representing depths up to 4.5 m. Sedimentary structures were described in the field and attention was given to bedding contacts and dip directions. Lithologic discontinuities are inferred through combined field description and laboratory identification of textural breaks and uniformity values of <2 mm fraction (e.g., Cremeens and Mokma, 1986; Schaetzl, 1998; Schaetzl and Anderson, 2005, p. 224). Munsell values are determined in the laboratory on moistened samples using a Konica Minolta CR-400 Chroma Meter.

To further describe sediments interpreted as aeolian for this study, micromorphological analysis was conducted on four, 5 × 7.5 cm thin sections from four stratigraphic sections (CB1a, GP5, U1, and U2; see **Figure 3** for locations). Micromorphology analysis follows established protocols and terminology (FitzPatrick, 1984; Stoops, 2003, 2010; Vepraskas and Wilson, 2008) with thin sections viewed through a polarizing microscope under plane polarized light (PPL), cross-polarized light (XPL), and oblique incident light (OIL). Thin section descriptions include compositional analysis of mineral grains through point counting within a 1 mm (horizontal) by 2 mm (vertical) grid system, similar to procedures suggested by FitzPatrick (1984, p. 104–106). This approach yields between 800 and 1000 potential mineral identifications per thin-section. Longest axial length and roundness, slightly modified from Powers (1953), are recorded for identified grains. When voids are encountered at observation points, the closest grain within 0.5 mm is selected for identification. Key micromorphological results are integrated within sedimentary discussions below.

Particle-size analysis is conducted via sieve-pipette method (Folk, 1974; Poppe et al., 2014). This study divides clay and silt at 4 μm. Statistics are calculated on grain size distributions including graphical median (*Md*) (Folk and Ward, 1957); first moment mean ($\bar{x}$), second moment standard deviation (σ), third moment skewness (*Sk*), fourth moment kurtosis (*K*) (Friedman, 1961; Pye and Tsoar, 2009, pp. 58–60); and coefficient of variation (*CV*) (Wong and Lee, 2005, p. 65). *Md*, $\bar{x}$, σ, *Sk*, and *K* statistics are calculated using Gradistat V.8 software (Blott and Pye, 2001) and results are presented using categories defined by Blott and Pye (2001). To facilitate comparison with previous studies (e.g., Leigh, 1998), *CV* is calculated for grain-size data using phi (Φ) units and are provided as percentages. Sedimentary facies are delineated based on consideration of statistical results, particle-size cumulative graphs, geomorphic and stratigraphic context, and OSL ages.

RESULTS

Aeolian Landforms and Sediments on the S2 Surface

Aeolian landforms and sediments on the S2 surface are restricted to elevations above 166 m, a conclusion that supports earlier findings (Morris and Pierce, 1967). Above 166 m is an array of hummocky landforms dominated by sandy sediments of variable thickness. Complex, linear, barchan-like and climbing dunes; an interdune sand sheet; and sand-mantled ridges are identified (**Figure 3**). A distinctive S2 landform above 166 m is a 1.06 km^2, low-relief, closed oval basin with complex dunes rimming most of its western margin (**Figure 3**). This low-relief basin is incised up to 9 m by Gilpin Run, a local tributary.

Average aeolian dune heights increase west to east, from 3 m immediately east of U.S. Route 52 to up to 9 m adjacent to the S2-S3 escarpment boundary (**Figure 3**). Planar cross-beds typically are encountered starting at ∼1 m or deeper in dunes, although some as shallow as 0.4 m are documented (**Figures 4**, **5**). The linear and climbing dunes contain both high-angle (>20°) and low-angle planar cross-beds with ENE to N and NNE dip directions, respectively. Sand-mantled ridges are restricted to west of U.S. Route 52 and include sand-textured, unstratified sediments unconformably overlaying

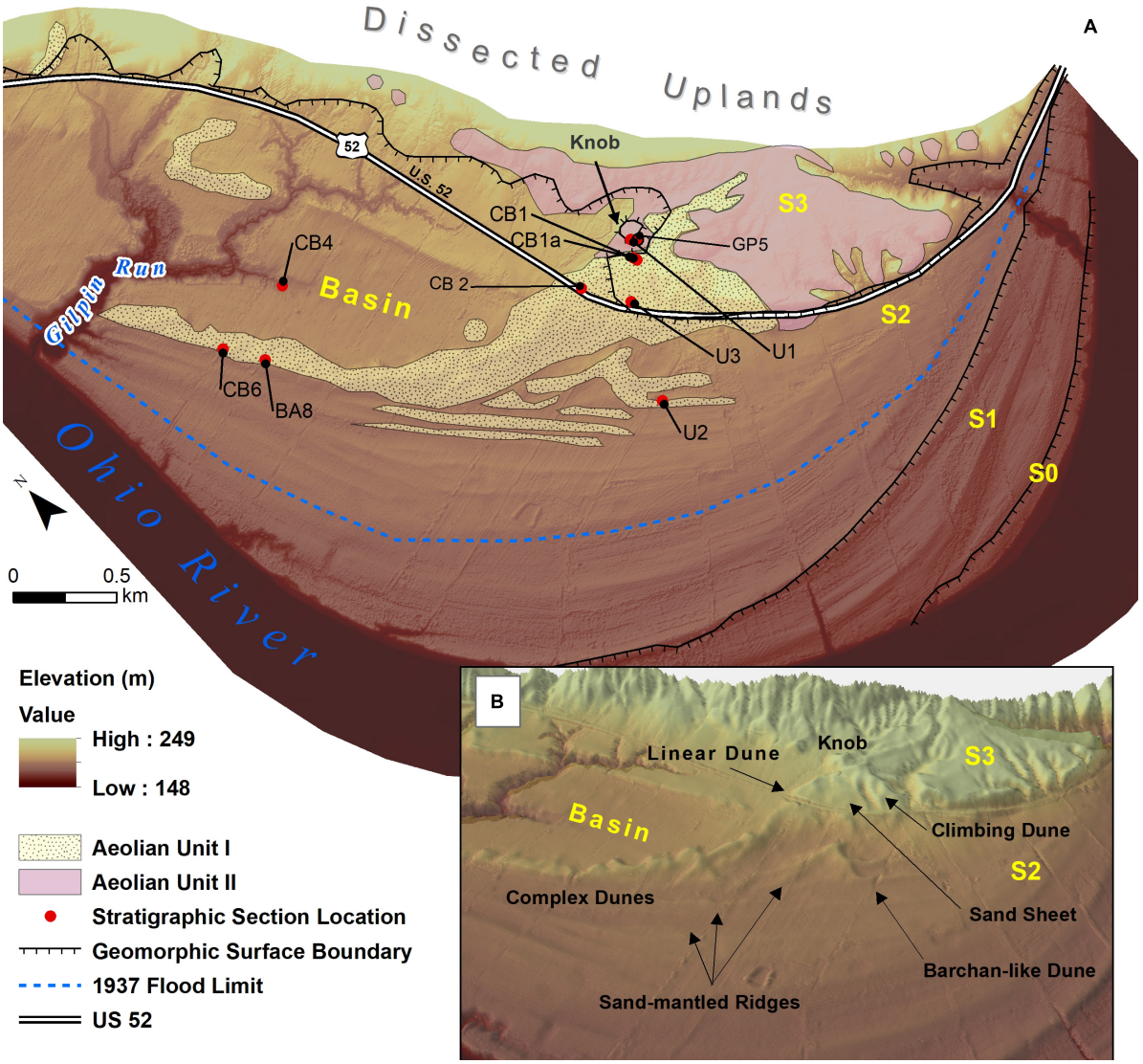

FIGURE 3 | (A) Sandy Springs LiDAR image showing distribution of described sections, geomorphic surfaces (S0-S3) and landforms, 1937 flood limit, and surficial distribution of aeolian units I and II. The distribution of aeolian units is based on current study results and previous research (Morris and Pierce, 1967). **(B)** Oblique ArcScene 3D representation of a close-up section of LiDAR image **(A)** at 3x vertical exaggeration showing dune types, interdunal sand sheet, and sand-mantled ridges.

fine-textured alluvial ridge crests. Sand-textured units range in thickness between 0.4 and 2 m. Buried paleosols are absent from dunes but secondary, pedogenic lamellae start at depths as shallow as ∼0.6 m in the bachan-like and linear dunes (**Figure 4**). A pedogenic interpretation for lamellae formation in these dunes is supported in thin-section where limpid, microlaminated clay is observed in lamellae bands (**Figure 6**). Under XPL, clay domains in lamellae exhibit high birefringence and optical continuity with straight extinction lines during microscope stage rotation. The pedogenic process of illuviation is the primary means by which such alignment and continuity occurs in clay domains (Stephen, 1960; Fedoroff, 1974; Stoops, 2003, p. 19).

Four lithostratigraphic facies were delineated for this study including aeolian units I and II and alluvial units I and II (**Tables 1**, **2** and **Figure 7**). An 'indeterminate' unit also is applied to samples not readily classified into one of the four facies. Alluvial unit I sediments represent the basal unit on the S2 landform and are moderately sorted, matrix-supported, low-angle cross-stratified sand and gravels interpreted as fluvioglacial outwash. The <2 mm fraction of this facies are a sandy mud or muddy sand texture ($\bar{x}$ = 72 μm), has symmetrical skew, are platykurtic, and have an average *CV* of 84.8% (**Table 2**). Sediments range in color from reddish (8.4 YR) to yellowish brown (9.5 YR) hues. Intact fluvioglacial deposits only were encountered in the S2 basin. Twenty historic water-well logs in

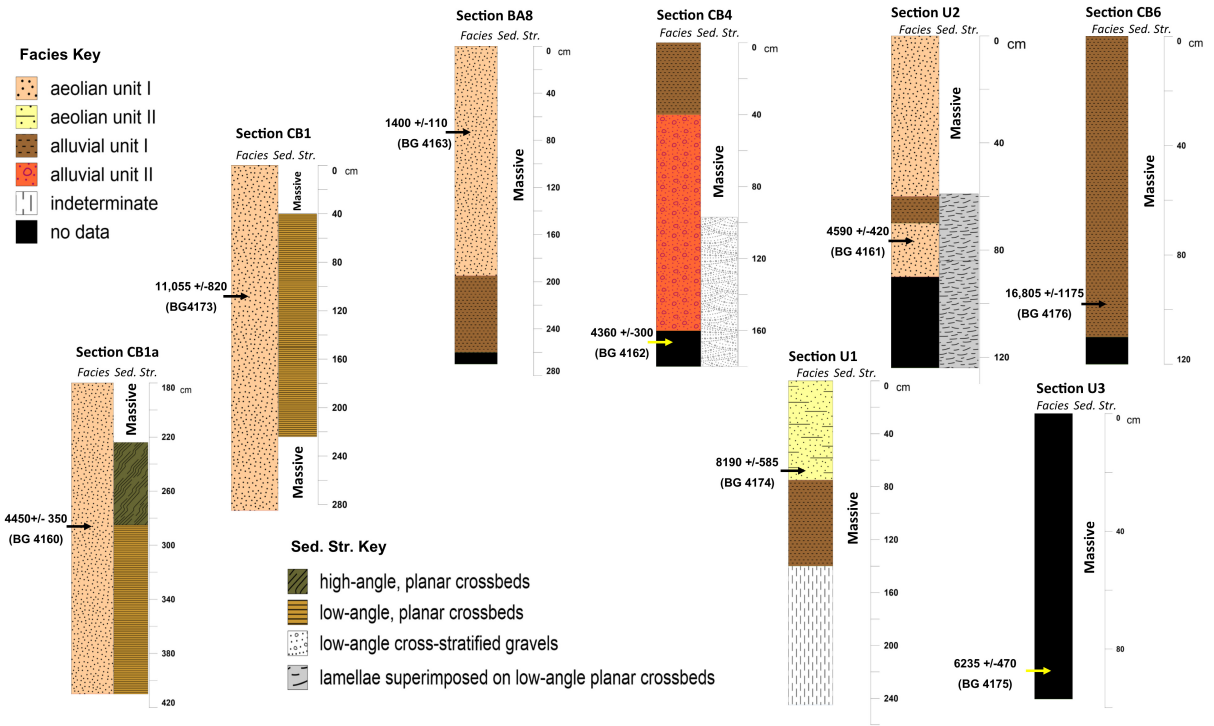

FIGURE 4 | Stratigraphic sections showing facies, sedimentary structures, and OSL age estimates. Section locations illustrated in **Figure 3**.

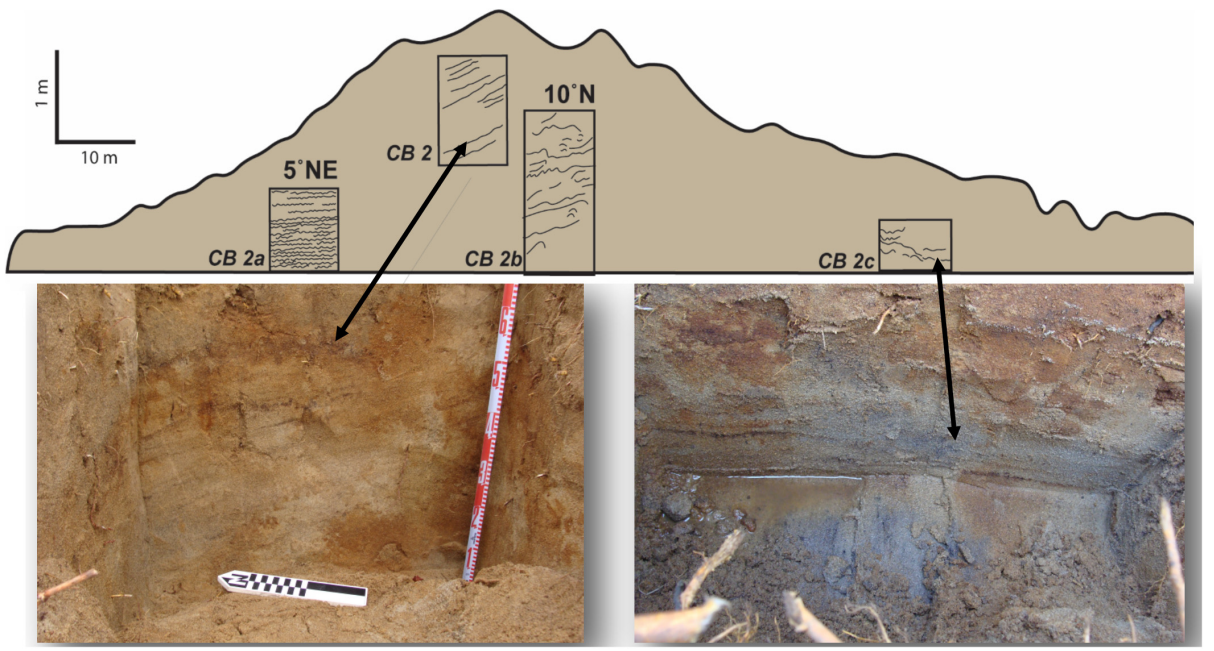

FIGURE 5 | Examples of primary planar cross-beds showing true dip angle and direction in linear dune at U.S. Route 52 road cut for Section CB2.

the immediate area of Sandy Springs indicate coarse sand and gravels beginning at various depths, mostly > 2 m (ODNR, 2017), and reportedly are up to 45 m thick beneath the S2 and S3 surfaces (Morris and Pierce, 1967).

Fine-grained alluvial unit II sediments unconformably overlay alluvial unit I sediments and are interpreted as low-energy overbank deposits. Alluvial unit II sediments are extremely poorly sorted sandy mud or silty sand ($\bar{x}$ = 38 μm). They

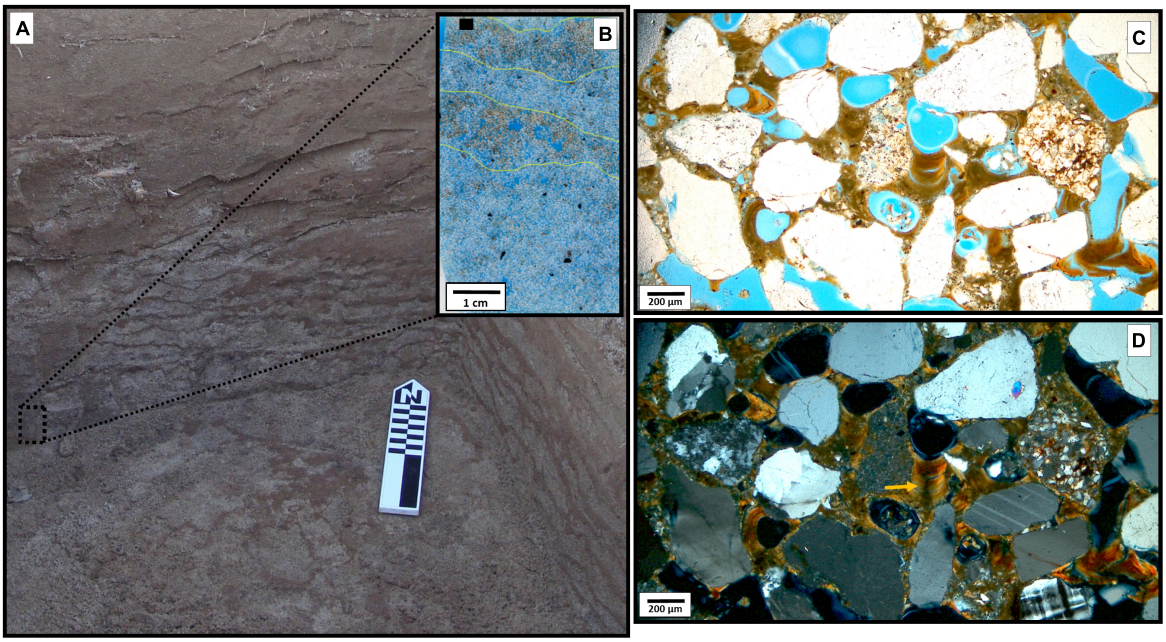

FIGURE 6 | (A) View of lamellae banding in barchan-like dune at ∼1 m depth, Section U2. **(B)** Scan of 5 × 7-cm thin section slide showing lamellae bands highlighted in yellow, black box represents approximate location of **(C,D)** (open pore space dyed blue). **(C)** PPL micrograph of well-oriented illuviated limpid clay domains linking grains in lamellae band. **(D)** same as **(C)** but in XPL, arrow denotes extinction line indicating continuous orientation of clay domains.

TABLE 1 | Particle-size characteristics by landform type for uppermost lithostratigraphic units (n = 89 samples).

Landform (surface)	Sample Size	*Md* (μm)	$\bar{x}$ (μm)	σ (μm)	*Sk*	*K*	*CV(%)*[a]
Barchan-like Dune (S2)	6	339	231	4.60	−3.26	13.75	99.5
Sand Dune, Linear Dune (S2)	8	362	279	3.77	−2.75	11.91	96.1
Sand Dune, Climbing Dune (S2)	4	346	260	3.71	−3.62	18.33	90.6
Sand Dune/Gully, Climbing Dune (S2)	5	271	108	6.20	−1.13	3.31	80.0
Sand Sheet (S2)	15	362	282	3.53	−3.11	14.60	90.8
Sand-mantled Ridges (S2)	9	214	144	7.06	−1.53	5.80	83.2
Knob (S3)	7	40	32	5.80	−0.70	2.79	49.8
Alluvial Ridge (S2)	5	35	20	7.64	−0.47	1.99	51.1
Alluvial Swale (S2)	1	350	233	4.45	−2.73	10.00	102.3
Alluvial Tread (S2)	18	26	16	7.54	−0.12	2.06	47.9
Tributary Drainage (S2)	11	22	16	6.36	−0.17	2.51	44.4

[a]*CV is calculated using phi (Φ) units of* $\bar{x}$ *and* σ.

exhibit a coarse skew, are mesokurtic, and have an average *CV* of 56.0% (**Table 2**). Sediments are reddish to yellowish brown with hues from 7.6 YR to 9.9 YR. Overbank deposits range in thickness between 1 m in the S2 basin to >4.5 m across the alluvial surface tread. The comparatively thin overbank deposits in the S2 basin, coupled with its low topographic relief, suggest fluvial and/or aeolian deflation of the basin floor.

Dune, sand-mantled ridge, and interdunal sand sheet sediments are delineated as aeolian unit I. These sands ($\bar{x}$ = 278 μm) are poorly sorted and exhibit a very coarse skew. They also are very leptokurtic and have an average *CV* of 83.0% (**Tables 1**, **2**). Sediments are brown to yellowish brown with hues from 8.1 YR to 0.8 Y. Micromorphological analysis indicate variation in grain morphologies with sub-rounded to sub-angular, low sphericity grain shapes being most common (52%) (**Table 3** and **Figure 6**). Only 7% of these grains are well-rounded with high sphericity. Grain sorting and texture properities suggest short-distance suspension, surface traction and saltation as primary sediment transport modes (Pye and Tsoar, 2009, pp. 113–115). The barchan-like dune and several of the sand-mantled ridges are interlayered with alluvial unit II and aeolian unit I sediments and are interpreted as reflecting fluvial-aeolian interaction.

Also revealed through micromorphology was the presence of sand-sized clay aggregates or pellets intermixed with mineral grains (e.g., quartz, chert, etc.). These clay pellets represent a significant portion of Aeolian Unit I grain assemblage (∼10%)

TABLE 2 | Particle-size description and characteristics by facies type (n = 163 samples).

Facies	Sample Size	General Description and Interpretation	*Md* (μm)	$\bar{x}$ (μm)	σ	*Sk*	*K*	*CV%*[a]
Aeolian unit I	85	Dunes and sand-mantled ridges, high and low angle planar cross beds and lamellae in dunes	346	278	3.54	−3.33	18.06	83.3
Aeolian unit II	9	Sandy loess, unstratified	39	31	5.35	−0.80	3.26	46.9
Alluvial unit I	5	Ohio River coarse-grained alluvium, gravel cross beds, interpreted as fluvioglacial outwash.	121	72	10.39	−0.39	2.53	84.8
Alluvial unit II	64	Ohio River fine-grained alluvium, rare laminated sands. Interpreted as overbank deposition.	72	38	7.22	−0.63	2.78	56.0

[a]*CV is calculated using phi (Φ) units of* $\bar{x}$ *and* σ.

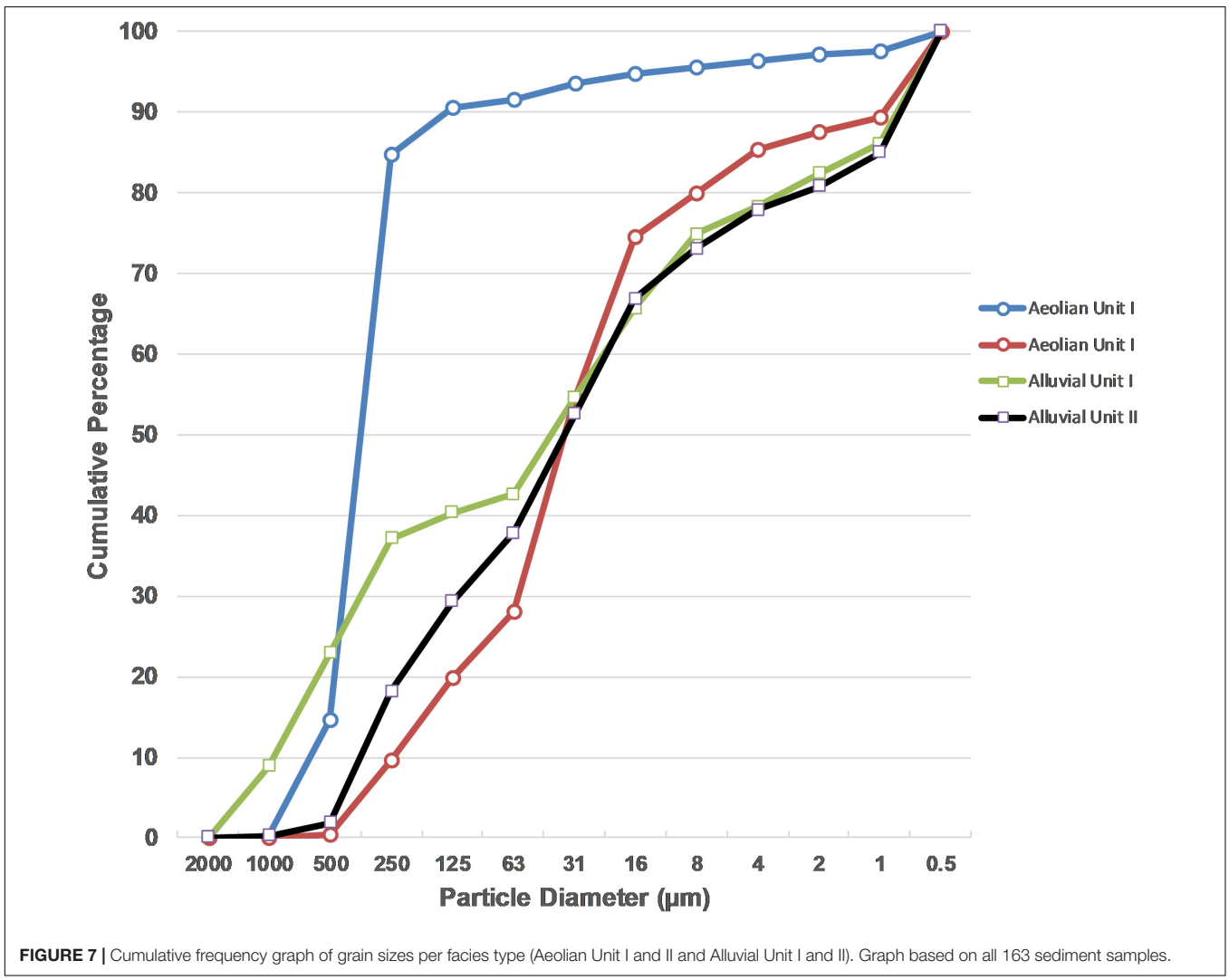

FIGURE 7 | Cumulative frequency graph of grain sizes per facies type (Aeolian Unit I and II and Alluvial Unit I and II). Graph based on all 163 sediment samples.

and are 'tempered' predominately with silt-sized quartz grains, although muscovite grains occur less frequently. Evidence of particle disaggregation and coalescing, reported as common by others (Mason et al., 2003, p. 383), is infrequent at Sandy Springs. Secondary (hydro)oxides impregnate some pellets. Clay pellets are commonly reported in central and eastern United States dune and loess deposits (e.g., Mason et al., 2003; Kilibarda and Blockland, 2011, pp. 309–310). Pelletization occurs under arid, or seasonally dry, conditions where wind erosion detaches and entrains the edges of mud curls or salt-mud efflorescences (Pye, 1987, p. 27; Pye and Tsoar, 2009, p. 93; Shaw and Bryant, 2011, p. 392). Effective pellet size (Stoops, 2003, p. 12) was measured in thin section on 181 specimens and pellets ranged in diameter between 160 and 1606 μm, with an average of coarse sand ($\bar{x}$ = 608 μm).

The timing of aeolian activity on the S2 surface is constrained by the OSL age of 16,805 ± 1175 (BG 4176; **Table 4**). This age estimate comes from silty overbank deposits that form an alluvial

TABLE 3 | Results of micromorphological analysis comparing grain compositions and morphologies between Aeolian Unit I and II facies at Sections U1, U2, GP5, and CB1a.

Grain Property		Aeolian Unit I	Aeolian Unit II
Q		91%	95%
C		6%	1%
F		2%	1%
M		<1%	2%
B/H		<1%	1%
Q:CA		7:1	197:1
Q:F		79:1	91:1
Grain Morphologies			
	Sub-angular, High Sphericity	9%	5%
	Sub-angular, Low Sphericity	12%	4%
	Sub-rounded, High Sphericity	22%	24%
	Sub-rounded, Low Sphericity	40%	52%
	Very Angular, High Sphericity	2%	0%
	Very Angular, Low Sphericity	2%	0%
	Well Rounded, High Sphericity	7%	8%
	Well Rounded, Low Sphericity	6%	7%

Q, quartz; C, chert; F, feldspar; M, muscovite; B, biotite; H, amphibole/hornblende; Q:CA, quartz:clay aggregate ratio; Q:F, quartz:feldspar ratio.

ridge crest that is unconformably overlain by ∼0.6 m of undated, sandier aeolian unit I sediments (Section CB6). The ∼17 ka age also supports previous suggestions that the S2 (O2) landform was constructed between 18 and 15 ka (Pavey et al., 1999). An OSL age estimate of 11,055 ± 820 (BG 4173; **Table 4**) from 1.25 m below the crest of the ∼9-m thick climbing dune, suggests dune formation was occurring on the S2 surface during the late Pleistocene, or between ∼17 and 11 ka.

OSL age estimates between ∼6.2 and 1.4 ka (BG 4160, BG 4161, BG 4163, BG 4175; **Table 4**) indicate continued aeolian activity during the Holocene on the S2 surface. An especially active time of landscape disturbance and aeolian sedimentation at Sandy Springs is indicated by OSL age estimates 4450 ± 350 (BG 4160), 4590 ± 420 (BG 4161), and 4360 ± 300 (BG 4162), all from different stratigraphic sections (**Table 4** and **Figure 3**). This clustering of ages at ∼4.5 ka suggest the occurrence of either closely timed, or synchronous, erosion, transport, and deposition events. Sample BG 4160 derives from the climbing dune, at a depth, 2.85 m, characterized by high-angle (>30°) planar cross-beds indicative of dune reactivation and grain flow on the NNE slip face. Dune reactivation may be associated with erosional undercutting and is further suggested by a high overdispersion equivalent dose value of 53 ± 5% (**Table 4**) that may indicate grain mixing (Galbraith et al., 1999). A second age (BG 4161) is from the limb section of the barchan-like dune and may reflect either initial dune/limb construction or subsequent reactivation. The final age (BG 4162) derives from a gully cut in the deflated S2 basin that exposes low-angle cross-stratified alluvial unit I sediments, and is interpreted as reflecting mid-Holocene reworking of older fluvioglacial deposits.

Aeolian Sediments on the S3 Surface

Abutting bedrock uplands to the east, the S3 surface is deeply eroded and rounded, especially along its western margin. The only portion of the S3 surface directly tested during this study is an isolated, erosional knob (**Figure 3**) that contains > 4.5 m of interlayered aeolian unit I, aeolian unit II, and alluvium unit I sediments. The upper 0.75 m of the knob is delineated as aeolian unit II. This unit represents an unstratified sandy loess that appears to blanket significant portions of the S3 surface beyond the knob landform (Morris and Pierce, 1967) (**Figure 3**) and is extremely poorly sorted sandy silt ($\bar{x} = 31\ \mu m$). The facies is characterized by a coarse skew, is mesokurtic, and has an average *CV* of 46.7% (**Tables 1**, **2**). Sediments are dark reddish brown with hues between 8.3 YR and 9.7 YR. Micromorphological analysis reveal common sub-rounded grain morphologies (76%) for this unit with only 8% well-rounded, high sphericity grain shapes (**Table 3**; see also **Figure 6**). Unlike Aeolian Unit I, Aeolian Unit II sediments contain few (<1%) clay pellets. Texture and sorting properities suggests modified saltation and short-distance suspension as primary transport modes (Pye and Tsoar, 2009, pp. 113–115). Although the S3 surface has been suggested to date to as early as the Illinoian, 160 ka (Morris and Pierce, 1967), and as late as the late Wisconsinan, 22 to 18 ka (Pavey et al., 1999), an OSL age estimate of 8190 ± 585 (BG 4174; **Table 4**) from 0.75 m in section U1 indicates Holocene sandy loess mantle portions of this surface.

DISCUSSION

Aeolian Landform Chronology and Evolution

Consistent with other upper Ohio Valley studies (Rutledge et al., 1975; Chappell, 1988; Simard, 1989), aeolian landforms and sediments at Sandy Springs are restricted to the older, elevated S2 and S3 landforms. On the S2 surface, aeolian sediments discontinuously cover a basal sequence of coarse fluvioglacial outwash, alluvial unit I, over fine overbank sediments, alluvial unit II. Fluvioglacial outwash was available for deposition at Sandy Springs perhaps as early as ∼23 ka, in association with the melting of the Scioto and Miami sublobes that delivered substantial meltwater and sediment to the Ohio River through the Scioto River (Kempton and Goldthwait, 1959; Fullerton, 1986; Glover et al., 2011). The relatively wide, sinuous, low-gradient Ohio valley between Garrison, Kentucky, and Sandy Springs (**Figure 1**) would have reduced river unit stream power and transport capacity (Leopold et al., 1964, pp. 271–317; Fryirs and Brierley, 2013, pp. 70–71) resulting in a sediment sink, especially at significant meanders such as Sandy Springs. OSL age results from this study indicate that the transition to fine overbank deposition and ridge-and-swale development on the S2 surface was in progress by at least ∼17 ka.

Sometime between 17 and 11 ka, aeolian processes commenced on the S2 surface. OSL age results indicate episodic aeolian deposition between 11 and 1.4 ka on both the S2 and S3 surfaces. Aeolian deposition appears to reflect both initial dune

TABLE 4 | Results of OSL dating for Sandy Springs.

Lab number	Section/ Depth (m)	Facies (Setting)[a]	Aliquots[b]	Grain Size (μm)	Equivalent dose (Gray)[c]	Overdis persion (%)[d]	U (ppm)[e]	Th (ppm)[e]	K (%)[e]	Cosmic dose rate (mGray/yr)	Dose rate (mGray/yr)[f]	OSL age (yr)[g]
BG 4160	CB1a/2.85	Aeolian unit I (climbing dune)	60/71/8	425–500	4.00 ± 0.23	53 ± 5	0.76 ± 0.01	1.72 ± 0.01	0.59 ± 0.01	0.160 ± 0.016	0.90 ± 0.05	4450 ± 350
BG 4161	U2/0.76	Mixed aeolian unit 1/alluvial unit 1(barchan-like dune)	61/70/10	425–355	7.82 ± 0.60	48 ± 4	2.04 ± 0.01	4.92 ± 0.01	088 ± 0.01	0.196 ± 0.020	1.72 ± 0.09	4590 ± 420
BG 4162	CB4/1.71	Alluvial unit I (alluvial surface tread)	51/63/9	425–355	7.58 ± 0.49	44 ± 4	1.83 ± 0.01	4.47 ± 0.01	1.05 ± 0.01	0.177 ± 0.018	1.74 ± 0.09	4360 ± 300
BG 4163	BA8/0.7	Aeolian unit I (alluvial ridge)	56/63/6	425–355	2.56 ± 0.13	40 ± 4	1.79 ± 0.01	2.88 ± 0.01	1.05 ± 0.01	0.198 ± 0.020	1.61 ± 0.08	1400 ± 110
BG 4173	CB1/1.25	Aeolian unit I (climbing dune)	41/51	425–355	10.53 ± 0.54	23 ± 3	0.77 ± 0.01	1.84 ± 0.01	0.58 ± 0.01	0.185 ± 0.019	0.95 ± 0.05	11,055 ± 820
BG 4174	U1/0.75	Aeolian II (knob)	32/35/9	355-250	14.10 ± 0.71	37 ± 5	2.00 ± 0.01	4. 41 ± 0.01	0.92 ± 0.01	0.192 ± 0.019	1.72 ± 0. 09	8190 ± 585
BG 4175	U3/0.85	Aeolian I (sand sheet)	28/35/6	425–355	7.43 ± 0.40	37 ± 5	1.13 ± 0.01	2.70 ± 0.01	0.69 ± 0.01	0.195 ± 0.020	1.19 ± 0.06	6235 ± 470
BG 4176	CB6/0.97	Alluvial unit II (alluvial ridge)	23/26	63-44	53.85 ± 2.62	21 ± 3	3.93 ± 0.01	11.10 ± 0.01	1.49 ± 0.01	0.192 ± 0.019	3.20 ± 0.16	16,805 ± 1175

[a]Facies units and Settings delineated in Section "Aeolian Sediments on the S3 Surface." [b]Aliquots used in equivalent dose calculations versus original aliquots measured. [c]Equivalent dose calculated on a pure quartz fraction with about 40–100 grains/aliquot and analyzed under blue-light excitation (470 ± 20 nm) by single aliquot regeneration protocols (Murray and Wintle, 2003). The central age model of Galbraith et al. (1999) was used to calculated equivalent dose when overdispersion values are <25% (at 1 sigma errors) A finite mixture age model was used with overdispersion values > 25% to determine the youngest equivalent dose population, which is the third value listed. [d]Values reflects precision beyond instrumental errors; values of ≤25% (at 1 sigma limit) indicate low dispersion in equivalent dose values and an unimodal distribution. [e]U, Th and K content analyzed by inductively coupled plasma-mass spectrometry analyzed by ALS Laboratories, Reno, NV; U content includes Rb equivalent. [f]Cosmic dose rate calculated from parameters in Prescott and Hutton (1994). [g]Systematic and random errors calculated in a quadrature at 1 standard deviation. Datum year is AD 2010.

construction and later reactivation events. The low frequency of well-rounded, high sphericity grains (8%) and extremely poor sediment sorting, along with overall high OSL overdispersion values (>30%) (Galbraith et al., 1999), are consistent with the view that aeolian sediments are locally sourced (Pye and Tsoar, 2009, p. 82). The proximity of the deflated S2 basin with aeolian dunes and sand-mantled ridges suggests that this depression represents a primary source area for aeolian sediments at Sandy Springs (**Figure 3**). The geographic position of complex dunes that partially rim the western edge of the basin also indicates source-bordering mechanisms which are common in sediment-rich alluvial valleys worldwide (e.g., Kocurek and Lancaster, 1999; Sankey et al., 2018). Aeolian deflation of this basin likely occurred in response to some combination of reduced vegetation cover, perhaps associated with increased aridity, and perhaps groundwater drawdown linked to the deep incision of Gilpin Run which concomitantly would have reduced water table elevations in the immediate area.

Aeolian deposits are thickest east of U.S. Route 52, where a linear dune transitions into a 9 m high climbing dune that abuts the S3 escarpment. The orientation and thickness of these cross-bedded dunes appear windswept and align closely with modern S to WSW seasonal wind regimes (National Climatic Data Center, 1996). The fact that S2 linear and climbing dunes, and the interdunal sand sheet, exhibit coarse textures ($\bar{x}$ < 302 μm) suggests winnowing of fines and subsequent deposition downwind on the S3 surface as fine-textured sandy loess ($\bar{x}$ = 31 μm) during the early Holocene. Based on the interlayering of aeolian unit I and alluvial unit II sediments, we interpret the formation of landforms west of U.S. Route 52 as a result of a more complex interplay of aeolian-fluvial processes interacting with the underlying alluvial topography. S2 alluvial ridge crests, for example, are shown in this study to be preferred points of deposition for up to 2 m of fine sandy sediment ($\bar{x}$ = 183 μm). In these cases, alluvial ridge crests act as promontories to decrease and redirect surface wind vectors and promote aeolian deposition (e.g., Dong et al., 2018).

Regional Comparisons and Possible Paleoclimate Correlations

Recent geochronological studies are yielding a growing inventory of <12 ka OSL and radiocarbon ages for aeolian landforms from a variety of geomorphic settings in the eastern United States (Hansen et al., 2002; Krieg et al., 2004; Lutz et al., 2007; Campbell et al., 2011; Kilibarda et al., 2014a). Most relevant to the current study are dated aeolian landforms such as dune fields located within alluvial valleys, paleochannels, or lake and outwash plains (e.g., Rawling et al., 2008; Miao et al., 2010; Kilibarda and Blockland, 2011; Wang et al., 2012; Blockland, 2013; Arbogast et al., 2015). In these settings, dunes typically are vegetated today and most commonly are reported to be transgressive parabolic and sand sheet forms. Similar to Sandy Springs, individual dunes heights vary but most are less than 15 m in height (Rawling et al., 2008, p. 495; Miao et al., 2010, p. 764; Kilibarda and Blockland, 2011, p. 307; Blockland, 2013, pp. 27–32).

In the eastern United States, evidence of Holocene aeolian deposition predominately is interpreted as reactivation and resculpting of the upper sections of extant late Pleistocene dunes (Miao et al., 2010; Blockland, 2013), an interpretation largely favored for Sandy Springs. Similar to dunes at Sandy Springs, most <12 ka age samples from aeolian landforms derive from shallow <2 m deposits, although early ages from depths between 5 and 7 m also are reported (Arbogast and Packman, 2004; Rawling et al., 2008; Miao et al., 2010; Kilibarda and Blockland, 2011; Wang et al., 2012; Arbogast et al., 2015, 2017). At least one dune in Illinois, the Bill Farm site, has OSL age estimates suggesting construction entirely during the Holocene (Miao et al., 2010, p. 768). At Sandy Springs, OSL age estimates suggest that S2 sand mantles and the barchan-like dune also were constructed primarily during the Holocene (**Table 4**). Although buried paleosols are currently unknown in aeolian contexts at Sandy Springs, their occurrence at other sites in Illinois, Ohio, and Wisconsin (Rawling et al., 2008; Miao et al., 2010; Wang et al., 2012; Blockland, 2013) suggests depositional hiatuses were common over the last 12 ka years in the eastern United States.

The formation of late Quaternary aeolian landforms has been attributed to a combination of factors including environmental change, notably increased aridity (Miao et al., 2010; Campbell et al., 2011; Kilibarda and Blockland, 2011), increased sediment supply (e.g., Arbogast et al., 2015), and increased sediment availability through groundwater drawdown and surface deflation (e.g., Rawling et al., 2008; Miao et al., 2010). Although not widely studied, local disturbances also may be responsible for site-specific reactivations such as animal overgrazing, wildfires, and Native American land-use practices (Miao et al., 2010, p. 770). Although local wind fetch and sediment availability are interpreted as important factors for initiating aeolian processes at Sandy Springs, OSL dating and internal dune architecture also suggest at least two possible linkages of local landscape instability to pan-regional Holocene paleoclimate events.

First, the OSL age estimate of ∼8.2 ka from sandy loess on the S3 surface indicates early Holocene deposition. Although based on a single age, we suggest the possibility that this depositional event is related to the 8.2 ka paleoclimate event, or North Atlantic Bond Event 5 (Bond et al., 1997). The 8.2 ka event reflects an abrupt centennial-scale cooling and drying episode characterized by increased windiness that appears related to North Atlantic sea-surface cooling due to the collapse of the Laurentide Ice Sheet (e.g., Alley et al., 1997; Bond et al., 1997; Hu et al., 1999; Yu and Eicher, 2001; Shuman et al., 2002; Alley and Ágústsdóttir, 2005; Ellison et al., 2006; Kobashi et al., 2007; Li et al., 2007). In North America specifically, increased dust frequencies in lacustrine sediments have been cited as evidence for intensifying aeolian activity across the continental United States at this time (e.g., Hu et al., 1999; Fritz et al., 2001; Dean et al., 2002; Tornqvist et al., 2004; Lutz et al., 2007). Potential linkages to the 8.2 ka event are suggested from two additional Ohio sites. Coring of lacustrine sediments at northcentral Ohio's Brown's Lake reveal two distinct, organic-poor silt beds dated between 8.9 and 8.2 ka (Lutz et al., 2007), which is interpreted as evidence for increased aeolian activity. Aeolian reactivation of late Pleistocene

beach deposits and sand dunes in northwestern Ohio also is documented beginning ∼8.8 ka and may reflect an early onset of the 8.2 ka event (Campbell et al., 2011).

A second possible paleoclimate link is based on three OSL age estimates that suggest likely synchronous, wide-spread landscape instability and sediment reworking at ∼4.5 ka on the S2 surface at Sandy Springs. This age closely corresponds to a period of lower lake levels and increased aridity in northeastern to southeastern United States between 4.4 and 4.5 ka (Li et al., 2007, 2014; Stinchcomb et al., 2013) and slightly predates severe drought at ∼4.2 ka for midcontinental North America, as well as other portions of the Northern Hemisphere (e.g., Dean, 1997; Alley et al., 2003; Staubwasser et al., 2003; Booth et al., 2004, 2005). Drought conditions like those reported between 4.5 and 4.2 ka are known to result in severe landform degradation and initiation of aeolian processes, including dune reactivations across portions of North America (e.g., Mason et al., 1997, 2004; Forman et al., 2001). Evidence from Sandy Springs suggest that a similar set of processes may have been occurring in the upper Ohio Valley during this time.

CONCLUSION

At the Sandy Springs site, geomorphic, stratigraphic, and sedimentary observations, supported by eight OSL age estimates, are the basis for the first detailed description of an aeolian system in the upper Ohio Valley. Aeolian sediments are restricted to an intermediate S2 surface and higher S3 surface. OSL age estimates constrain the initial timing of S2 aeolian processes to between 17 and 11 ka. Episodic aeolian deposition on the S2 and S3 surfaces continued during the Holocene between 11 and 1.4 ka, with strong evidence of pervasive landscape disturbance and aeolian activity at ∼4.5 ka. S2 aeolian sediments primarily are medium-textured and form dunes and sand-mantled ridges; whereas, S3 deposits represent sandy loess that blankets an underlying, older surface. Aeolian sediments are interpreted as locally sourced. Hummocky terrain on the S2 surface east of U.S. Route 52 reflect stabilized dunes with cross-bedded sands of varied thickness. The depositional history of landforms west of U.S. Route 52 are more complex with evidence of fluvial-aeolian interaction. The timing of aeolian activity at Sandy Springs may indicate linkages to pan-regional Holocene paleoclimate events at 4.5 and 8.2 ka. Finally, the potential that Holocene aeolian sediments are distributed more broadly within the upper Ohio Valley has important implications not only for future landform and paleoenvironmental reconstructions, but also for late Quaternary archeological studies that explore issues of site preservation and visibility (e.g., Waters and Kuehn, 1996; Purtill, 2012).

DATA AVAILABILITY STATEMENT

The datasets generated for this study are available on request to the corresponding author.

AUTHOR CONTRIBUTIONS

MP and JK participated in field work and wrote and edited the text. SF conducted the OSL dating and wrote and edited portions of the text.

FUNDING

Geochronology and micromorphology work was supported by a 2016 NASA West Virginia Space Grant Consortium Graduate Research Fellowship.

ACKNOWLEDGMENTS

Various individuals provided project assistance including James Thompson and Kathy Benison of West Virginia University; Steve Baker of USDA-NRCS; Chris Bedel of the Edge of Appalachia Preserve System; Nancy Stranahan of the Arc of Appalachia; and Mike Angle, Frank Fugitt, and Nathan Erber of the Ohio Geological Survey. Field and laboratory assistance was provided by Francesca Basil; Andrew Braun; Nick Dadamo; Sara DeAloia; Nancy Gostic; Zach Haidar; Heather Jewel; Matt Koerner; Miles Reed; Emily Swaney; Katie Wasley; and Joey Zampayo. Finally, special thanks go to the Adams, Rutledge, and Whisman families for providing property access.

SUPPLEMENTARY MATERIAL

The Supplementary Material for this article can be found online at: https://www.frontiersin.org/articles/10.3389/feart.2019.00322/full#supplementary-material

REFERENCES

Aitken, M. J. (1998). *An Introduction to Optical Dating: The Dating of Quaternary Sediments by the Use of Photon-stimulated Luminescence*. Oxford: Clarendon Press.

Alley, R. B., and Ágústsdóttir, A. M. (2005). The 8k event: cause and consequences of a major Holocene abrupt climate change. *Quat. Sci. Rev.* 24, 1123–1149. doi: 10.1016/j.quascirev.2004.12.004

Alley, R. B., Marotzke, J., Nordhaus, W. D., Overpeck, J. T., Peteet, D. M., Pielke, R. A., et al. (2003). Abrupt climate change. *Science* 299, 2005–2010. doi: 10.1126/science.1081056

Alley, R. B., Mayewski, P. A., Sowers, T., Stuiver, M., Taylor, K. C., and Clark, P. U. (1997). Holocene climatic instability: a prominent, widespread event 8200 yr ago. *Geology* 25, 483–486.

Arbogast, A. F., Hansen, E. C., and Van Oort, M. D. (2002). Reconstructing the geomorphic evolution of large coastal dunes along the southeastern shore of Lake Michigan. *Geomorphology* 46, 241–255. doi: 10.1016/S0169-555X(02)00076-4

Arbogast, A. F., Luehmann, M. D., Miller, B. A., Wernette, P. A., Adams, K. M., Waha, J. D., et al. (2015). Late-Pleistocene paleowinds and aeolian sand mobilization in north-central lower Michigan. *Aeolian Res.* 16, 109–116. doi: 10.1016/j.aeolia.2014.08.006

Arbogast, A. F., Luehmann, M. D., William Monaghan, G., Lovis, W. A., and Wang, H. (2017). Paleoenvironmental and geomorphic significance of bluff-top dunes along the Au Sable River in northeastern lower Michigan, USA. *Geomorphology* 297, 112–121. doi: 10.1016/j.geomorph.2017.09.017

Arbogast, A. F., and Packman, S. C. (2004). Middle-Holocene mobilization of aeolian sand in western upper Michigan and the potential relationship with climate and fire. *Holocene* 14, 464–471. doi: 10.1191/0959683604hl723rr

Bettis, E. A., Muhs, D. R., Roberts, H. M., and Wintle, A. G. (2003). Last glacial loess in the conterminous USA. *Quat. Sci. Rev.* 22, 1907–1946. doi: 10.1016/s0277-3791(03)00169-0

Blockland, J. D. (2013). *The surficial geology of Fulton County, Ohio: insight into the late Pleistocene-early Holocene glaciated landscape of the Huron-Erie Lake Plain, Fulton County, Ohio, USA*. Master Thesis, The University of Toledo, Toledo.

Blott, S. J., and Pye, K. (2001). GRADISTAT: a grain size distribution and statistics package for the analysis of unconsolidated sediments. *Earth Surf. Process. Landforms* 26, 1237–1248. doi: 10.1002/esp.261

Bond, G., Showers, W., Cheseby, M., Lotti, R., Almasi, P., DeMenocal, P., et al. (1997). A pervasive millennial-scale cycle in North Atlantic Holocene and glacial climates. *Science* 278, 1257–1266. doi: 10.1126/science.278.5341.1257

Booth, R. K., Jackson, S. T., Forman, S. L., Kutzbach, J. E., Bettis, E. A., Kreig, J., et al. (2005). A severe centennial-scale drought in midcontinental North America 4200 years ago and apparent global linkages. *Holocene* 15, 321–328. doi: 10.1191/0959683605hl825ft

Booth, R. K., Jackson, S. T., and Gray, C. E. D. (2004). Paleoecology and high-resolution paleohydrology of a kettle peatland in upper Michigan. *Quat. Res.* 61, 1–13. doi: 10.1016/j.yqres.2003.07.013

Brockman, C. S. (2006). *Physiographic Regions of Ohio*. Columbus: Department of Natural Resources.

Busacca, A. J., Beget, J. E., Markewich, H. W., Muhs, D. R., Lancaster, N., and Sweeney, M. R. (2004). "Aeolian sediments," in *The Quaternary Period in the United States, Developments in Quaternary Science*, eds A. R. Gillespie, and S. C. Porter, (Amsterdam: Elsevier), 275–309.

Campbell, M. C., Fisher, T. G., and Goble, R. J. (2011). Terrestrial sensitivity to abrupt cooling recorded by aeolian activity in northwest Ohio, USA. *Quat. Res.* 75, 411–416. doi: 10.1016/j.yqres.2011.01.009

Chaplin, J. R., and Mason, C. E. (1967). *Geologic map of the Garrison Quadrangle, Kentucky-Ohio, and part of the Pond Run Quadrangle, Lewis County, Kentucky*. Kentucky: U.S. Geological Survey.

Chappell, G. A. (1988). *Identification and Correlation of the Fluvial Terraces in the Ohio River Valley Near Proctorville*. Madison: Ohio and Cox Landing.

Coogan, A. H. (1996). *Ohio's Surface Rocks and Sediments. Ohio Divis*. Columbus: Ohio Department of Natural Resources.

Cremeens, D. L., and Mokma, D. L. (1986). Argillic horizon expression and classification in the soils of two Michigan hydrosequences. *Soil Sci. Soc. Am. J.* 50, 1002–1007. doi: 10.2136/sssaj1986.03615995005000040034x

Daniel, I. R. Jr., Moore, C. R., and Caynor, E. C. (2013). Sifting the sands of time: geoarchaeology, culture chronology, and climate change at Squires Ridge, northeastern North Carolina. *Southeast. Archaeol.* 32, 253–270. doi: 10.1179/sea.2013.32.2.006

Dean, W. E. (1997). Rates, timing, and cyclicity of Holocene eolian activity in north-central United States: evidence from varved lake sediments. *Geology* 25, 331–334.

Dean, W. E., Forester, R. M., and Bradbury, J. P. (2002). Early Holocene change in atmospheric circulation in the northern Great Plains: an upstream view of the 8.2 ka cold event. *Quat. Sci. Rev.* 21, 1763–1775. doi: 10.1016/S0277-3791(02)00002-1

Dong, M., Yan, P., Liu, B., Wu, W., Meng, X., Ji, X., et al. (2018). Distribution patterns and morphological classification of climbing dunes in the Qinghai-Tibet Plateau. *Aeolian Res.* 35, 58–68. doi: 10.1016/j.aeolia.2018.09.002

Ellison, C. R. W., Chapman, M. R., and Hall, I. R. (2006). Surface and deep ocean interactions during the cold climate event 8200 years ago. *Science* 312, 1929–1932. doi: 10.1126/science.1127213

Feathers, J. K., Rhodes, E. J., Huot, S., and Mcavoy, J. M. (2006). Luminescence dating of sand deposits related to late Pleistocene human occupation at the Cactus Hill site, Virginia, USA. *Quat. Geochronol.* 1, 167–187. doi: 10.1016/j.quageo.2006.05.011

Fedoroff, N. (1974). "Classification of accumulations of translocated particles," in *Soil Microscopy*, ed. G. K. Rutherford, (Kingston: Limestone Press), 695–700.

FitzPatrick, E. A. (1984). *The Micromorphology of Soils*. London: Chapman and Hall.

Folk, R. L. (1974). *Petrology of Sedimentary Rocks*. Austin: Hemphill Publishing Company.

Folk, R. L., and Ward, W. C. (1957). Brazos River bar: a study in the significance of grain size parameters. *J. Sediment. Res.* 27, 3–26. doi: 10.1306/74d70646-2b21-11d7-8648000102c1865d

Forman, S. L. (2015). Episodic eolian sand deposition in the past 4000 years in Cape Cod National Seashore, Massachusetts, USA in response to possible hurricane/storm and anthropogenic disturbances. *Front. Earth Sci.* 3:3. doi: 10.3389/feart.2015.00003

Forman, S. L., Oglesby, R., and Webb, R. S. (2001). Temporal and spatial patterns of holocene dune activity on the Great Plains of North America: megadroughts and climate links. *Glob. Planet. Change* 29, 1–29. doi: 10.1016/s0921-8181(00)00092-8

Fredlund, G. G. (1989). *Holocene Vegetational History of the Gallipolis Locks and Dam Project Area, Mason County, West Virginia*. Lexington: Cultural Resource Analysts, Inc.

Friedman, G. M. (1961). Distinction between dune, beach, and river sands from their textural characteristics. *J. Sediment. Res.* 31, 514–529.

Fritz, S. C., Metcalfe, S. E., and Dean, W. (2001). "Holocene climate patterns in the Americas inferred from paleolimnological records," in *Interhemispheric Climate Linkages*, ed. V. Markgraf (Boulder: Academic Press), 241–263. doi: 10.1016/B978-012472670-3/50018-5

Fryirs, K. A., and Brierley, G. J. (2013). *Geomorphic Analysis of River Systems: An aAproach to Reading the Landscape*. Oxford: John Wiley & Sons.

Fullerton, D. S. (1986). Stratigraphy and correlation of glacial deposits from Indiana to New York and New Jersey. *Quat. Sci. Rev.* 5, 23–37. doi: 10.1016/0277-3791(86)90171-x

Galbraith, R. F., Roberts, R. G., Laslett, G. M., Yoshida, H., and Olley, J. M. (1999). Optical dating of single and multiple grains of quartz from Jimmum Rock Shelter, northern Austrailia: part I, experimental design and statistical models. *Archaeometry* 41, 339–364. doi: 10.1111/j.1475-4754.1999.tb00987.x

Glover, K. C., Lowell, T. V., Wiles, G. C., Pair, D., Applegate, P., and Hajdas, I. (2011). Deglaciation, basin formation and post-glacial climate change from a regional network of sediment core sites in Ohio and eastern Indiana. *Quat. Res.* 76, 401–410. doi: 10.1016/j.yqres.2011.06.004

Hansen, E., Arbogast, A., Packman, S., and Hansen, B. (2002). Post-Nipissing origin of a backdune complex along the southeastern shore of Lake Michigan. *Phys. Geogr.* 23, 233–244. doi: 10.2747/0272-3646.23.3.233

Hanson, P. R., Mason, J. A., Jacobs, P. M., and Young, A. R. (2015). Evidence for bioturbation of luminescence signals in eolian sand on upland ridgetops, southeastern Minnesota, USA. *Quat. Int.* 362, 108–115. doi: 10.1016/j.quaint.2014.06.039

Hu, F. S., Slawinski, D., Wright, H. E., Ito, E., Johnson, R. G., Kelts, K. R., et al. (1999). Abrupt changes in North American climate during early Holocene times. *Nature* 400, 437–440. doi: 10.1038/22728

Ivester, A. H., and Leigh, D. S. (2003). Riverine dunes on the coastal plain of Georgia, USA. *Geomorphology* 51, 289–311. doi: 10.1016/S0169-555X(02)00240-4

Ivester, A. H., Leigh, D. S., and Godfrey-Smith, D. I. (2001). Chronology of inland eolian dunes on the coastal plain of Georgia, USA. *Quat. Res.* 55, 293–302. doi: 10.1006/qres.2001.2230

Jones, R. R. (1916). *The Ohio River: Charts, Drawings, and Description of Features Affecting Navigation*. Washington, D.C: Government Printing Office.

Kempton, J. P., and Goldthwait, R. P. (1959). Glacial outwash terraces of the Hocking and Scioto River valleys, Ohio. *Ohio J. Sci.* 59, 135–151.

Kilibarda, Z., and Blockland, J. (2011). Morphology and origin of the Fair Oaks dunes in NW Indiana, USA. *Geomorphology* 125, 305–318. doi: 10.1016/j.geomorph.2010.10.011

Kilibarda, Z., Venturelli, R., and Goble, R. (2014a). "Late Holocene dune development and shift in dune-building winds along southern Lake Michigan," in *Coastline and Dune Evolution along the Great Lakes*, eds T. G. Fisher, and E. C. Hansen, (Boulder: Geological Society of America), 47–64.

Kilibarda, Z., Venturelli, R., and Goble, R. J. (2014b). Late Holocene dune development and shift in dune-building winds along southern Lake Michigan. *Pap. Earth Atmos. Sci.* 421, 1–19.

Kobashi, T., Severinghaus, J. P., Brook, E. J., Barnola, J. M., and Grachev, A. M. (2007). Precise timing and characterization of abrupt climate change 8200 years ago from air trapped in polar ice. *Quat. Sci. Rev.* 26, 1212–1222. doi: 10.1016/j.quascirev.2007.01.009

Kocurek, G., and Lancaster, N. (1999). Aeolian system sediment state: theory and Mojave Desert delso dune field example. *Sedimentology* 46, 505–515. doi: 10.1046/j.1365-3091.1999.00227.x

Krieg, J. R., Bettis, E. A., and Forman, S. L. (2004). Evidence for late Holocene eolian sand reactivation in the Green River Lowland, northwestern Illinois; regional response to drought and potential implications. *Geol. Soc. Am.* 36:70.

Lancaster, N. (2011). "Desert dune processes and dynamics," in *Arid Zone Geomorphology: Process, Form and Change in Drylands*, ed. D. S. G. Thomas, (Oxford: Wiley-Blackwell), 487–515. doi: 10.1002/9780470710777.ch19

Leigh, D. S. (1998). Evaluating artifact burial by eolian versus bioturbation processes, South Carolina Sandhills, USA. *Geoarchaeology* 13, 309–330. doi: 10.1002/(sici)1520-6548(199802)13:3<309::aid-gea4>3.0.co;2-8

Leopold, L. B., Wolman, M. G., and Miller, J. P. (1964). *Fluvial Processes in Geomorphhology*. New York, NY: Dover Publications, Inc.

Li, Y.-X., Yu, Z., and Kodama, K. P. (2007). Sensitive moisture response to Holocene millennial-scale climate variations in the Mid-Atlantic region, USA. *Holocene* 17, 3–8. doi: 10.1177/0959683606069386

Li, Z.-H., Driese, S. G., Stinchcomb, G. E., Kocis, J. J., Horn, S. P., Buckles, J., et al. (2014). "Earlier onset of "4.2 KA Event" in the Eastern U.S. is possible at 4.5 KA: middle Holocene mega-droughts identified using stable isotopes and micromorphology of speleothems and δ13C of floodplain SOM," in *Proceedings of the Speleotherm Records of Climate Change in North America*, (Vancouver: GSA Annual Meeting).

Lothrop, J. C., and Cremeens, D. L. (2010). 33Ms391: a Paleoindian site in southwestern Ohio. *Curr. Res. Pleistocene* 27, 120–122.

Lucht, T. E., and Brown, D. L. (1994). *Soil Survey of Adams County, Ohio*. Columbus: United States Department of Agriculture - Soil Conservation Service.

Lutz, B., Wiles, G., Lowell, T., and Michaels, J. (2007). The 8.2-ka abrupt climate change event in Brown's Lake, Northeast Ohio. *Quat. Res.* 67, 292–296. doi: 10.1016/j.yqres.2006.08.007

Markewich, H. W., Litwin, R. J., Wysocki, D. A., and Pavich, M. J. (2015). Synthesis on Quaternary aeolian research in the unglaciated eastern United States. *Aeolian Res.* 17, 139–191. doi: 10.1016/j.aeolia.2015.01.011

Mason, J. A., Jacobs, P. M., Greene, R. S. B., and Nettleton, W. D. (2003). Sedimentary aggregates in the peoria loess of Nebraska, USA. *Catena* 53, 377–397. doi: 10.1016/S0341-8162(03)00073-0

Mason, J. A., Swinehart, J. B., Goble, R. J., and Loope, D. B. (2004). Late-Holocene dune activity linked to hydrological drought, Nebraska Sand Hills, USA. *Holocene* 14, 209–217. doi: 10.1191/0959683604hl677rp

Mason, J. P., Swinehart, J. B., and Loope, D. B. (1997). Holocene history of lacustrine and marsh sediments in a dune-blocked drainage, southwestern Nebraska Sand Hills, U.S.A. *J. Paleolimnol.* 17, 67–83. doi: 10.1023/A:1007917110965

Miao, X., Hanson, P. R., Wang, H., and Young, A. R. (2010). Timing and origin for sand dunes in the Green River lowland of illinois, upper Mississippi River valley, USA. *Quat. Sci. Rev.* 29, 763–773. doi: 10.1016/j.quascirev.2009.11.023

Morris, R. H., and Pierce, K. L. (1967). *Geologic Map of the Vanceburg Quadrangle, Kentucky-Ohio*. Reston: U S Geological survey.

Muhs, D. R., and Zárate, M. (2001). "Late Quaternary eolian records of the Americas and their paleoclimatic significance," in *Interhemispheric Climate Linkages*, ed. V. Markgraf, (New York, NY: Academic Press), 183–216. doi: 10.1016/b978-012472670-3/50015-x

Murray, A. S., and Wintle, A. G. (2003). The single aliquot regenerative dose protocol: potential for improvements in reliability. *Radiat. Meas.* 37, 377–381. doi: 10.1016/S1350-4487(03)00053-2

National Climatic Data Center (1996). *Climatic Wind Data for the United States: 1930-1996*. Available at: https://www.ncdc.noaa.gov (accessed July 4, 2017).

NOAA (2017). *National Weather Service. River Observations*. Available at: http://water.weather.gov (accessed January 6, 2017).

ODNR (2017). *ODNR Division of Water Resources*. Available at: http://water.ohiodnr.gov/search-file-well-logs (accessed January 1, 2017).

OGRIP (2015). *Ohio Geographically Referenced Information Program*. Available at: http://ogrip.oit.ohio.gov/ (accessed June 6, 2015).

Pavey, R. R., Goldthwait, R. P., Brockman, C. S., Hull, D. N., Swinford, E. M., and Van Horn, R. G. (1999). *Quaternary Geology of Ohio*. Columbus: State of Ohio, Department of Natural Resources.

Peel, M. C., Finlayson, B. L., and McMahon, T. A. (2007). Updated world map of the köppen-geiger climate classification. *Hydrol. Earth Syst. Sci.* 11, 1633–1644. doi: 10.5194/hess-11-1633-2007

Poppe, L. J., McMullen, K. Y., Williams, S. J., and Paskevich, V. F. (2014). *USGS East-Coast Sediment Analysis: Procedures, Database, and GIS Data*. Reston: U S Geological survey.

Powers, M. C. (1953). A new roundness scale for sedimentary particles. *J. Sediment. Res.* 23, 117–119. doi: 10.1306/D4269567-2B26-11D7-8648000102C1865D

Prescott, J. R. R., and Hutton, J. T. T. (1994). Cosmic ray contributions to dose rates for luminescence and esr dating: large depths and long-term time variations. *Radiat. Meas.* 23, 497–500. doi: 10.1016/1350-4487(94)90086-8

Purtill, M. P. (2012). *A Persistent Place: A Landscape Approach to the Prehistoric Archaeology of the Greenlee Tract in Southern Ohio*. Raleigh: Lulu Press, Inc.

Purtill, M. P. (2016). "Aeolian and fluvial interaction in the middle Ohio River valley: new geomorphic, stratigraphic, and sedimentological evidence from sandy springs, adams county, Ohio," in *Proceedings of the Geological Society of America Abstracts with Programs*, Denver, CO.

Purtill, M. P. (2017). Reconsidering the potential role of saline springs in the paleoindian occupation of sandy springs, adams county, Ohio. *J. Archaeol. Sci. Rep.* 13, 164–174. doi: 10.1016/j.jasrep.2017.03.054

Purtill, M. P., and Kite, J. S. (2015). "Midwestern sand dunes, geoarchaeology, and lidar: preliminary geomorphic landform analysis of the sandy springs paleoindian site in the upper Ohio River valley," in *Proceedings of the Geological Society of America Abstracts with Programs*, (Madison: Geological Survey of India). doi: 10.1016/j.jasrep.2017.03.054

Pye, K. (1982). Morphological development of coastal dunes in a humid tropical environment, cape bedford and cape flattery, North Queensland. *Geogr. Ann. A.Physical Geogr.* 64A, 213–227. doi: 10.1080/04353676.1982.11880067

Pye, K. (1987). *Aeolian Dust and Dust Deposits*. London: Academic Press.

Pye, K., and Tsoar, H. (2009). *Aeolian Sand and Sand Dunes*. Berlin: Springer.

Rawling, J. E., Hanson, P. R., Young, A. R., and Attig, J. W. (2008). Late Pleistocene dune construction in the central sand plain of Wisconsin, USA. *Geomorphology* 100, 494–505. doi: 10.1016/j.geomorph.2008.01.017

Rittenour, T. M., Blum, M. D., and Goble, R. J. (2007). Fluvial evolution of the lower Mississippi River valley during the last 100 k.y. glacial cycle: response to glaciation and sea-level change. *Bull. Geol. Soc. Am.* 119, 586–608. doi: 10.1130/B25934.1

Rodbell, D. T., Forman, S. L., Pierson, J., and Lynn, W. C. (1997). Stratigraphy and chronology of Mississippi valley loess in western Tennessee. *Bull. Geol. Soc. Am.* 109, 1134–1148. doi: 10.1130/0016-7606(1997)109<1134:sacomv>2.3.co;2

Rutledge, E. M., Holowychuk, N., Hall, G. F., and Wilding, L. P. (1975). Loess in Ohio in relation to several possible source areas: I. physical and chemical properties. *Soil Sci. Soc. Am. J.* 39, 1125–1132. doi: 10.2136/sssaj1975.03615995003900060031x

Sankey, J. B., Kasprak, A., Caster, J., East, A. E., and Fairley, H. C. (2018). The response of source-bordering aeolian dunefields to sediment-supply changes 1: effects of wind variability and river-valley morphodynamics. *Aeolian Res.* 32, 228–245. doi: 10.1016/j.aeolia.2018.02.005

Saucier, R. T. (1977). Sand dunes and related aeolian features of the lower Mississippi River alluvial valley. *Geosci. Man* 19, 23–40.

Schaetzl, R. J. (1998). Lithologic discontinuities in some soils on drumlins: theory, detection, and application. *Soil Sci.* 163, 570–590. doi: 10.1097/00010694-199807000-00006

Schaetzl, R. J., and Anderson, S. (2005). *Soils: Genesis and Geomorphology*. Cambridge: Cambridge University Press.

Shaw, P. A., and Bryant, R. G. (2011). "Pans, Playas and Salt Lakes," in *Arid Zone Geomorphology: Process, Form and Change in Drylands*, ed. D. S. G. Thomas, (Oxford: Wiley-Blackwell), 373–401. doi: 10.1002/9780470710777.ch15

Shuman, B., Webb, T. III, Bartlein, P., and Williams, J. W. (2002). The anatomy of a climatic oscillation: vegetation change in eastern North America during the

younger dryas chronozone. *Quat. Sci. Rev.* 21, 1777–1791. doi: 10.1016/s0277-3791(02)00030-6

Simard, C. M. (1989). *Geologic History of the Lower Terraces and Floodplains of the Upper Ohio River Valley*. Morgantown: West Virginia Geological & Economic Survey.

Slucher, E. R., Swinford, E. M., Larsen, G. E., Schumacher, G. A., Shrake, D. K., Rice, C. K., et al. (2006). *Bedrock Geologic Map of Ohio, BG-1, Version 6*.

Staubwasser, M., Sirocko, F., Grootes, P. M., and Segl, M. (2003). Climate change at the 4.2 ka bp termination of the Indus valley civilization and Holocene south asian monsoon variability. *Geophys. Res. Lett.* 30, 1425–1428. doi: 10.1029/2002GL016822

Stephen, I. (1960). Clay orientation in soils. *Sci. Prog.* 48, 322–331.

Stinchcomb, G. E., Messner, T. C., Williamson, F. C., Driese, S. G., and Nordt, L. C. (2013). Climatic and human controls on Holocene floodplain vegetation changes in eastern Pennsylvania based on the isotopic composition of soil organic matter. *Quat. Res.* 79, 377–390. doi: 10.1016/j.yqres.2013.02.004

Stoops, G. (2003). *Guidelines for Analysis and Description of Soil and Regolith Thin Sections*. Madison: Soil Science Society of America.

Stoops, G. (2010). *Interpretation of Micromorphological Features of Soils and Regoliths*. Oxford: Elsevier.

Swezey, C. S., Fitzwater, B. A., Whittecar, G. R., Mahan, S. A., Garrity, C. P., González, W. B. A., et al. (2016). The carolina sandhills: Quaternary eolian sand sheets and dunes along the updip margin of the Atlantic Coastal Plain province, southeastern United States. *Quat. Res.* 86, 271–286. doi: 10.1016/j.yqres.2016.08.007

Thomas, D. S. G. (2011). "Aeolian landscapes and bedforms," in *Arid Zone Geomorphology: Process, Form and Change in Drylands*, ed. D. S. G. Thomas, (Oxford: Wiley-Blackwell), 427–454.

Thornthwaite, C. W. (1931). The climate of north america according to a new classification. *Geogr. Rev.* 21, 633–655.

Thorson, R. M., and Schile, C. A. (1995). *Deglacial Eolian Regimes in New England*, Vol. 107. Washington, DC: Geological Society of America Bulletin.

Tornqvist, T. E., Bick, S. J., Gonzalez, J. L., van der Borg, K., and de Jong, A. F. M. (2004). Tracking the sea-level signature of the 8.2 ka cooling event: new constraints from the Mississippi delta. *Geophys. Res. Lett.* 31:L23309.

USDA-NRCS (2017). *Web Soil Survey. USDA-NRCS*. Available at: http://websoilsurvey.nrcs.usda.gov/. (accessed January 7, 2017).

Vepraskas, M. J., and Wilson, M. A. (2008). "Soil micromorphology: concepts, techniques, and applications," in *Methods of Soil Analysis: Part 5 - Mineralogical Methods*, eds A. L. Ulery, and L. R. Drees, (Madison: American Society of Agronomy), 191–226.

Vincent, M. A., Gardner, R. L., and Riley, B. P. (2011). Additions to and interesting records for the Ohio vascular flora (with one new record for indiana). *Phytoneuron* 60, 1–23.

Wagner, D. P., and McAvoy, J. M. (2004). Pedoarchaeology of Cactus Hill, a sandy paleoindian site in southeastern Virginia, U.S.A. *Geoarchaeology* 19, 297–322. doi: 10.1002/gea.10120

Wang, H., Curry, B., Stumpf, A., Miao, X., Waninger, S., Hanson, P., et al. (2011). "Evidence of regional drought from dune and loess records during the early stage of LIS retreat in the midwestern United States," in *Proceedings of the AGU Fall Meeting*, (San Francisco: American Geophysical Union).

Wang, H., Stumpf, A. J., Miao, X., and Lowell, T. V. (2012). Atmospheric changes in North America during the last deglaciation from dune-wetland records in the midwestern United States. *Quat. Sci. Rev.* 58, 124–134. doi: 10.1016/j.quascirev.2012.10.018

Waters, M. R., and Kuehn, D. D. (1996). The Geoarchaeology of place: the effect of geological processes on the preservation and interpretation of the archaeological record. *Am. Antiq.* 61, 483–497. doi: 10.2307/281836

Wells, G. L. (1983). "Late-glacial circulation over central North America revealed by Aeolian Features," in *Variations in the Global Water Budget*, eds F. A. Street-Perrott, M. Beran, and R. Ratcliffe, (Oxford: Springer), 317–330. doi: 10.1007/978-94-009-6954-4_25

Willard, D. A., Bernhardt, C. E., Korejwo, D. A., and Meyers, S. R. (2005). Impact of millennial-scale Holocene climate variability on eastern North American terrestrial ecosystems: pollen-based climatic reconstruction. *Glob. Planet. Change* 47, 17–35. doi: 10.1016/j.gloplacha.2004.11.017

Wong, D. W. S., and Lee, J. (2005). *Statistical Analysis of Geographic Information with ArcView GIS and Arcgis*. Hoboken: Wiley.

Yu, Z., and Eicher, U. (2001). Three amphi-atlantic century-scale cold events during the Bølling-Allerød warm period. *Géogr. Phys. Quat.* 55, 171–179. doi: 10.7202/008301ar

Conflict of Interest: The authors declare that the research was conducted in the absence of any commercial or financial relationships that could be construed as a potential conflict of interest.